Reconstruction of Mixed Boundary Objects and Classification Using Deep Learning and Linear Sampling Method

Shimoga Beerappa HARISHA, Erramshetty MALLIKARJUN, Magdum AMIT

Dept. of Electronics and Communication Engineering, National Institute of Technology, Goa, Farmagudi, Ponda, India

harishasb@jnnce.ac.in, emallikarjuna@nitgoa.ac.in, amitmagdum7671@gmail.com

Submitted January 9, 2024 / Accepted April 16, 2024 / Online first April 30, 2024

Abstract. *The linear sampling method is a simple and reliable linear inversion technique for determining the morphological features of unknown objects under investigation. Nevertheless, there are many challenges that this method depends on the frequency of operation and it is unable to produce satisfactory results for objects with complex shapes. This paper proposes a hybrid model, which combines conventional linear sampling method and deep learning for the reconstruction of mixed boundary objects. In this approach, the initial approximation of mixed boundary objects derived from linear sampling method serves as the training data for the U-Net based convolutional neural network. The network then learns to correlate this approximation with the corresponding ground truth profiles. Along with the reconstruction of mixed boundary objects, they are also classified as dielectric or conductor, and count of each object type are measured. Furthermore, the low-frequency and high-frequency characteristics of the linear sampling method are analyzed, and its limitations are overcome by combining it with a deep learning approach. The effectiveness of the proposed model is validated using several examples of synthetic and experimental data. The results demonstrate that the proposed method outperforms the conventional Linear sampling method in terms of accuracy.*

Keywords

Deep learning, linear sampling method, mixed boundary objects, microwave imaging

1. Introduction

Microwave imaging (MI) has great potential for the detection and precise localization of objects in remote or inaccessible locations. It is widely applied in various domains, such as nondestructive testing, geophysical exploration, biomedical imaging and diagnosis, through-wall imaging, remote sensing, security checks, and others [1], [2].

Among qualitative microwave imaging methods, Linear sampling method (LSM) [3] stands out as the simple, reliable, and effective tool. Furthermore, LSM has demonstrated successful applications in detecting coated objects, buried objects, objects concealed behind walls, and even identifying breast cancer cells [4–9]. In [10], LSM was employed for microwave breast cancer imaging (MBI) and led to the development of a device known as "SAFE" (Scan and Find Early) designed for the early detection of breast cancer. Linear sampling method was employed in all of these works, where the targets were treated as either dielectric or perfect electric conducting (PEC) objects. In [11], the analysis of LSM behavior in mixed boundary cases is presented, taking into account parameters such as operating frequency and permittivity. The study reported the following findings: 1) Regarding frequency, LSM exhibits dissimilar characteristics compared to dielectrics and perfect electric conductors (PEC). Specifically, at low frequencies, linear sampling method can only detect perfect electric conductor materials and is unable to detect dielectrics. 2) At very high frequencies, the quality of reconstruction significantly deteriorates.

Deep learning is emerging as a dominant tool for providing precise and reliable solutions in the field of microwave imaging, yet maintaining computational efficiency [12–14]. A deep learning-based approach in conjugation with the Fourier diffraction theorem is proposed in [15] to solve the inverse scattering problem encountered in quantitative microwave imaging (MWI). In [16], the orthogonality sampling method (OSM) is used along with deep learning architecture called the U-Net to reconstruct the permittivites of the dielectric objects. In [17], a deep learning-assisted linear sampling method (DLSM) is proposed for the reconstruction of multi-layered dielectric objects with cylindrical and rectangular cross-sections. So far, this is the only work reported on LSM with deep learning. In [18], a unified learning-based approach is introduced to solve inverse scattering problems (ISPs) with mixed boundary conditions. The scattering behavior of hybrid dielectric and perfect electric conductors (PEC) scatterers is modeled by the T-matrix method. A rough image of the zero-order T-matrix coefficients for unknown

DOI: 10.13164/re.2024.0299

scatterers is firstly reconstructed by the back-propagation method, which is then refined by an attention-assisted pix2pix generative adversarial network. In [19] A physics-inspired neural network named APU-Net is designed to solve Inverse Scattering Problems with mixed boundary conditions. The input to the APU-Net is derived from the back-propagation method. A neural network method is used to realize the alternate iterative update of parameters, thus separating the reconstruction of the PEC part from the DIE part.

The novelty of the paper lies in the proposed hybrid model, which combines conventional LSM and deep learning to reconstruct mixed boundary objects. deep learning is also employed to elevate the capabilities of linear sampling method reconstruction by addressing its limitations, such as its inability to reconstruct dielectrics at low frequencies (200 MHz) and significant deterioration in reconstruction quality at very high frequencies (8 GHz) are also addressed using deep learning. Further investigation involves classifying objects as either perfect electric conductors or dielectric and determining the number of PEC and dielectric objects within the area of interest. The proposed deep learning-assisted LSM for the reconstruction of mixed boundary objects is validated using various examples of synthetic and experimental data, namely 'FoamMeExt', provided by the Fresnel Institute [20]. The results demonstrate that the proposed method outperforms state-of-the-art reconstruction techniques in reconstructing mixed boundary objects.

This paper is organized as follows. The problem formulation is covered in Sec. 2, LSM algorithm is briefed in Sec. 2.1 and deep learning based linear sampling method for inverse problem of mixed boundary objects is discussed in Sec. 2.2. Comparison with the related method is discussed in Sec. 2.3. Thereafter, numerical results for various testing examples are reported in Sec. 3.1 for 3 GHz. The comparison of results is done in Sec. 3.2. The low frequency and high frequency characteristics of LSM is discussed in Sec. 3.3 and 3.4 respectively. As a final point in the result section, the classification of PEC / dielectric is reported in Sec. 3.5. Finally, Section 4 contains the concluding remarks.

2. Problem Formulation

The typical two-dimensional scalar electromagnetic scattering issue [21] is taken into consideration for numerical simplicity. As depicted in Fig. 1, the dielectric and perfect electric conductors objects have been placed in a domain Ω. The objects dimensions along the z-axis are taken to be infinite. The Π and θ represents the domains of PEC and dielectric objects respectively. The permittivity and the permeability of the dielectric objects are ϵ and μ respectively. These objects are surrounded by a background medium of permittivity ϵ_b and permeability μ_b. When the objects are exposed to a TM-polarized wave emitted by a transmitting antenna ($\mathrm{T_x}$), the integral forms of the equations for the total field and scattered field can be expressed as [22]:

$$u\left(\underline{r}\right) = u^{\mathrm{inc}}\left(\underline{r}\right) - \mathrm{j}\omega\mu_\mathrm{b}\int_{\mathrm{PEC}} G\left(\underline{r},\underline{t}^{'}\right) I^{\mathrm{c}}\left(\underline{t}^{'}\right)\mathrm{d}\underline{t}^{'} - \mathrm{j}\omega\mu_\mathrm{b},$$
$$\int_{\mathrm{Die}} G\left(\underline{r},\underline{r}^{'}\right) I^{\mathrm{p}}\left(\underline{r}^{'}\right)\mathrm{d}\underline{r}^{'},\ \underline{t}^{'}\in\partial\Pi,\ \underline{r}^{'}\in\Theta,\ \underline{r}\in(\partial\Pi,\Theta), \tag{1}$$

$$u^{\mathrm{scat}}\left(\underline{r}\right) = -\mathrm{j}\omega\mu_\mathrm{b}\int_{\mathrm{PEC}} G\left(\underline{r},\underline{t}^{'}\right) I^{\mathrm{c}}\left(\underline{t}^{'}\right)\mathrm{d}\underline{t}^{'} - \mathrm{j}\omega\mu_\mathrm{b}$$
$$\int_{\mathrm{Die}} G\left(\underline{r},\underline{r}^{'}\right) I^{\mathrm{p}}\left(\underline{r}^{'}\right)\mathrm{d}\underline{r}^{'},\ \underline{t}^{'}\in\partial\Pi,\ \underline{r}^{'}\in\Theta,\ \underline{r}\in\Gamma. \tag{2}$$

The Cartesian coordinates of the object domain and measurement domain are given by $\underline{r}^{'} = (x^{'}, y^{'}) = \underline{t}^{'}$ and $\underline{r} = (x, y)$, respectively. Γ is the measurement domain and ω is the angular frequency. u^{inc}, u^{scat}, and u are the incident field, scattered field and total field, respectively. I^{c} represents the impressed conduction current density associated with the boundary conditions of PEC. I^{p} represents the polarization current density and is related to the properties of dielectric objects by

$$I^{\mathrm{p}} = \mathrm{j}\omega(\epsilon - \epsilon_\mathrm{b})u = \mathrm{j}\omega\epsilon_\mathrm{b}\chi u \tag{3}$$

where $\chi = (\epsilon_\mathrm{r} - 1)$ is the contrast function and ϵ_r is the relative permittivity given by $\epsilon_\mathrm{r} = \epsilon/\epsilon_\mathrm{b}$. Here, all electric fields and induced current densities have only one component, i.e., the component along the longitudinal direction of the objects ($\hat{z}$) and may be considered as scalar quantities. G is the scalar Green's function for the homogeneous background, defined as:

$$G\left(\underline{r},\underline{t}^{'}\right) = \frac{1}{4\mathrm{j}}H_0^{(2)}\left(k_\mathrm{b}\left|\underline{r}-\underline{t}^{'}\right|\right) \tag{4}$$

where $H_0^{(2)}(.)$ is the Hankel function of second kind and zeroth order and k_b is the wave number.

For a PEC, induced currents exist solely along the boundary ($\partial\Pi$), while in the case of dielectrics, these currents are distributed throughout the entire dielectric region (Θ). If $\underline{r}\in\partial\Pi$, then u becomes zero, whereas u is nonzero if $\underline{r}\in\Theta$ and it is related to I^{p} by (3). Hence, equations (1) and (2) need to be solved to compute u^{scat} at different receiver ($\mathrm{R_x}$) positions within Γ. This process can be accomplished using the method of moments (MoM) [23], which involves the initial discretization of the integral equations, followed by the solution of a system of linear equations to determine the unknown values (I^{c}, I^{p}, u^{scat}). Further mathematical intricacies can be referenced in [22]. In the proposed method, 24 transceivers are used and located uniformly on a circular measurement domain of 0.6 m radius. Furthermore, the domain of investigation (DOI) measuring 20 cm × 20 cm is discretized to 40 × 40.

2.1 Linear Sampling Method

The LSM offers an estimation of the target's support by addressing an auxiliary linear inverse problem, instead of the nonlinear problem presented in (1) and (2). In the context of the aforementioned scenario, this auxiliary problem is represented as [3]:

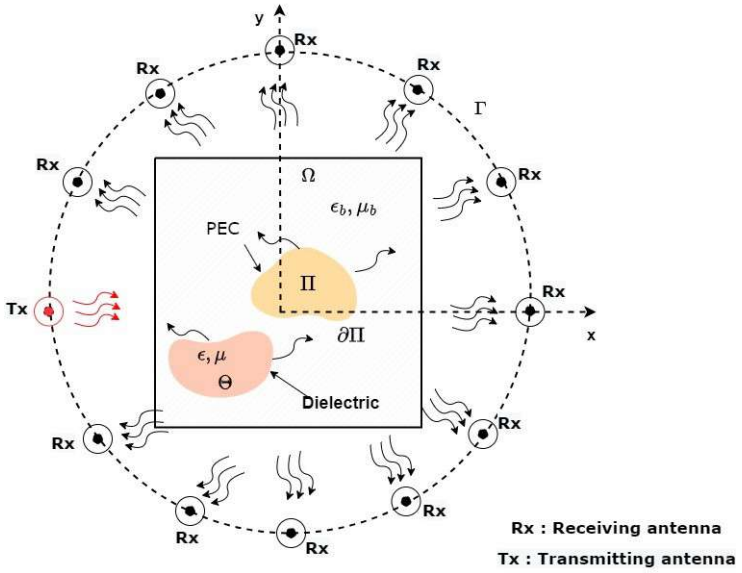

Fig. 1. Two-dimensional measurement configuration.

$$\mathcal{F}[\xi] = \int_0^{2\pi} u^{\text{scat}}\left(\underline{r}, \theta_{\text{i}}\right) \xi\left(\underline{r}_{\text{s}}, \theta_{\text{i}}\right) \mathrm{d}\theta_{\text{i}} = G\left(\underline{r}, \underline{r}_{\text{s}}\right) \tag{5}$$

where G is the point source, $\underline{r}_{\text{s}} \in \Omega$ denotes a point of an arbitrary grid that samples the region under test Ω, ξ is the unknown to be determined, the objects are illuminated by an incident field from a direction θ_{i}, the scattered fields are measured at a far-field distance $\underline{r}$ and $\mathcal{F} : L^2(\Gamma) \rightarrow L^2(\Gamma)$ is the far-field operator [21].

In order to estimate the support of the scatterers, the auxiliary linear equation (5) needs to be solved for each value of $\underline{r}_{\text{s}}$. According to the linear sampling method, the solution, in the form of energy $\left\|\xi(\underline{r}_{\text{s}})\right\|^2$, remains bounded if $\underline{r}_{\text{s}}$ corresponds to the scatterer support and becomes unbounded otherwise [3]. In this context, $\|\cdot\|$ represents the standard L^2-norm. Consequently, equation (5) is considered ill-posed [24] and requires regularization to ensure a stable solution. Further mathematical intricacies can be referenced in [3], [25]. The final form of the regularized solution, employing the singular value decomposition (SVD) technique [1], can be expressed as follows:

$$\left\|\xi(\underline{r}_{\text{s}})\right\|^2 = \sum_{n=1}^{N} \left(\frac{\lambda_n}{\lambda_n^2 + \alpha^2}\right)^2 |f \cdot \mu_n|^2 \tag{6}$$

where λ_n and μ_n are singular values and left singular vector of $\mathcal{F}$, respectively. ξ is the vector of unknowns, vector f is the farfield pattern radiated by the point source located at $\underline{r}_{\text{s}}$, N is the total number of nonzero singular values, and α is a regularization parameter. Therefore, the support of the scatterer is found by plotting $\left\|\xi(\underline{r}_{\text{s}})\right\|^2$ over the investigating domain. In the standard implementation of linear sampling method, α is estimated for each $\underline{r}_{\text{s}}$ using generalized discrepancy principle [3]. To enhance computational efficiency, previous studies in [6, 9, 26, 27] have demonstrated that a single regularization parameter can be applied to all sampling points. A smaller rho (optimized regularization parameter) value typically results in a smoother reconstruction, as it imposes stronger regularization, effectively suppressing noise but potentially sacrificing fine details of the object. On the other hand, a larger rho value allows for a more faithful reconstruction of intricate features but may lead to increased sensitivity to noise in the data. In this research, this parameter is computed based on physics-based criteria, as detailed in [6], eliminating the need for information about the noise level present in the measured data. Regularization parameter is set as $\alpha = 0.0001\lambda_1$, where λ_1 is the leading singular value.

2.2 Deep Learning Assisted Linear Sampling Method for Inverse Problem of Mixed Boundary Objects

Deep learning has emerged as one of the most effective techniques for solving regression and classification challenges in recent years. These results have encouraged researchers to use deep learning to address a range of challenges, including inverse problems. Deep learning techniques, compared to traditional iterative methods based on optimization, are significantly faster and yield higher-quality images [28]. Motivated by the results of our previous research on applying linear sampling method and deep learning to reconstruct PEC objects [29], a similar U-Net architecture [30] as shown in Fig. 2 is used to improve LSM's reconstruction performance, especially for objects with mixed boundaries and complex shapes. Convolutional layers and max-pooling layers make up the encoder portion of the U-Net. These layers gradually decrease the spatial dimensions while increasing the number of feature maps. The decoder part consists of convolutional layers followed by upsampling layers, which upsample the feature maps to the original input resolution while decreasing the number of channels. Better reconstruction is aided by the merging of low-level and high-level fea-

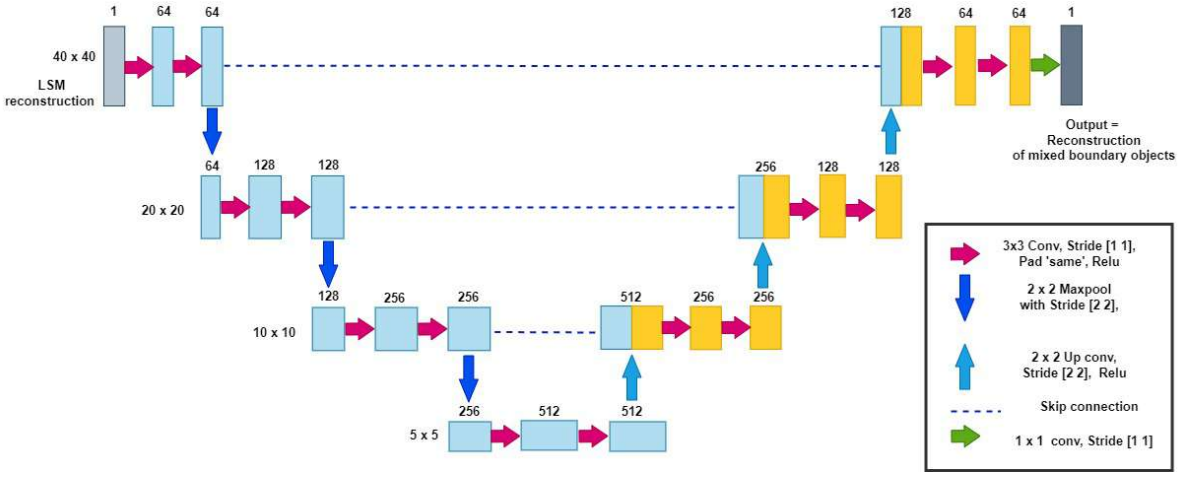

Fig. 2. Architecture details of U-Net for the proposed model.

tures made possible by the skip connections between relevant encoder and decoder levels. More details about the U-Net architecture used in this work can be found in [17], [29].

Let I_{g}^{i} represent the ground truth of the i^{th} mixed boundary object. The i^{th} reconstructed result from the U-Net is represented as I_{p}^{i}. U-Net is trained to reconstruct the groundtruth I_{g}^{i}, given the initial guess obtained from the reconstruction by linear sampling method. The loss function L is defined as the mean squared error between the predicted result I_{p}^{i} and the ground truth I_{g}^{i}:

$$L = \frac{1}{N} \sum_{i=1}^{i=N} \left\| I_{\mathrm{p}}^{i} - I_{\mathrm{g}}^{i} \right\|^{2} \tag{7}$$

where N is the number of training examples.

The loss function L is minimized with respect to the parameters of the U-Net model. Weights and biases of the U-Net are updated using backpropogation and an Adam optimization algorithm. By training the U-Net using the LSM reconstruction as input and groundtruth object profiles as output, the network learns to improve the LSM reconstructions and produce more accurate results. This integrating combines the strengths of both LSM and deep learning techniques for better reconstruction of mixed boundary objects.

The U-Net is trained using 4550 mixed boundary objects with various shapes, such as circular cylinders, rectangles, L-shape, and U-shape. The scattered field of these objects is computed by using 24 transceivers. The reconstruction obtained by linear sampling method is used as the training input, and the original profile serves as the label to train the U-Net. The DOI is discretized into 40×40 pixels. The detection domain is presumed to have a background of free space, with the contrast function set to zero.

The network is trained with the mean square error (MSE) as a loss function, and the parameters are tuned using the adaptive moment estimation (Adam) optimizer with a learning rate of 0.0001. Convolutional neural network (CNN) is trained for 60 epochs with 130 iterations per epoch and a batch size of 35. In addition, 0.5 dropout regularization is used to prevent over-fitting. Elapsed time for training is 169 minutes 2 seconds in a personal computer with CPU: 12th Gen Intel(R) Core(TM) i7-12700 2.10 GHz and 16 GB RAM. The U-Net learns the relationship between input and output by updating network's weight matrix and bias. The trained U-Net is tested for various unknown mixed boundary objects. As the background of DOI is assumed to be free space, negative values in the reconstructed results are set to zero during post-processing. The next section discusses the various test results.

2.3 Comparison with Related Method

In [18], a unified learning-based approach is introduced to solve inverse scattering problems (ISPs) with mixed boundary conditions. The proposed model differs from the one proposed in [18] in several ways. Firstly, the proposed model consists of a U-Net CNN, whereas [18] used a generative adversarial network (GAN). GAN consists of two neural networks contesting with each other in a game. Given a training set, this technique learns to generate new data with the same statistics as the training set. However, as GANs are composed of two networks, each with its loss function, they are inherently unstable. Secondly, the input to the U-Net is derived from the linear sampling method, while [18] used the roughly reconstructed result back-propagation method. Thus, the proposed model differs from [18]. Thirdly, the proposed model is trained using basic circular and rectangular cylinders, whereas in [18], MNIST digits are used along with random circles incorporated into each digit for training. Therefore, our model has learned the relationship better. Fourthly, in [18], the relative errors of PEC and dielectric scatterers are separately defined by dividing the reference profile into two parts. However, in the proposed model, the reconstruction error is quantified differently. Here, it is characterized as the ratio between the number of misclassified pixels and the total number of pixels, providing a distinct approach to measuring error.

3. Results and Discussion

The imaging setup consists of a square investigation domain of side 20 cm × 20 cm. Mixed objects are reconstructed using the noisy scattered field. MATLAB's Deep Learning toolbox is used to build the U-Net architecture. The proposed scheme is tested for various test images. Here 24 transceivers are used, which are located uniformly on a circular measurement domain of 0.6 m radius. The operating frequency is 3 GHz. The scattered field of synthetic data have been corrupted with additive Gaussian noise at the level of a signal-to-noise ratio (SNR) of 30 dB.

To quantify the reconstruction error, the error is defined as the ratio of the number of misclassified pixels to the total number of pixels [31].

Computation of error is described as follows: Let $I_g(x, y)$ and $I_r(x, y)$ be the ground truth image and reconstructed image, respectively. Based on the threshold T_e, these images are mapped to I_{gmap} and I_{rmap} binary images [31] such that:

$$I_{gmap}(x, y) = \begin{cases} 1 & \text{if } I_g(x, y) > T_e, \\ 0 & \text{if } I_g(x, y) \leq T_e, \end{cases} \tag{8}$$

$$I_{rmap}(x, y) = \begin{cases} 1 & \text{if } I_r(x, y) > T_e, \\ 0 & \text{if } I_r(x, y) \leq T_e. \end{cases} \tag{9}$$

If the pixel value is greater than the threshold value T_e, then that pixel belongs to a scatterer. A misclassified pixel is either outside the scatterer, satisfying condition (9), or inside the scatterer, not satisfying the condition (9). The threshold T_e is defined as:

$$T_e = \min(I_{rmap}(x, y)) + S_e(\max(I_{rmap}(x, y) - \min(I_{rmap}(x, y)). \tag{10}$$

The scaling parameter S_e is set to 0.5 as defined in [32]. Now, the error is defined as [17]:

$$Error = \frac{\sum_{n=1}^{N_T} (I_{rmap} - I_{gmap})}{N_T} \tag{11}$$

where N_T is the total number of pixels.

The proposed scheme is tested for the various mixed objects and the reconstruction results for some representative examples are shown in Figs. 3–7. The error for these examples is presented in Tab. 1. The results reveal that the proposed method outperforms the LSM algorithm in reconstructing high-quality images.

3.1 The Reconstruction Results at 3 GHz

Example 1: In this example, a PEC cylinder of radius 2 cm centered at origin and two dielectric strips of $\epsilon_r = 1.5$ are considered. Each dielectric strip has length (horizontally) and breadth (vertically) of 14 cm and 2 cm, respectively, and is separated from the PEC object's center by 6 cm, as shown in Fig. 3(a). The reconstruction by linear sampling method and proposed method is shown in Fig. 3(b) and 3(c) respectively. The reconstruction error for LSM is 0.8150, whereas for the proposed method, it is significantly reduced to 0.0519. The results demonstrate that the CNN outperforms LSM reconstruction in terms of the shape, location, and size of the objects. linear sampling method fails to accurately reconstruct the edges of the objects, and this issue worsens, especially at the edges facing PEC objects.

Example 2: In this study, a PEC cylinder of radius 2 cm centred at (6 cm, 6 cm) along with an L-shape dielectric object is taken, as shown in Fig. 4(a). Each arm of the L-shape has length and breadth of 14 cm and 3 cm, respectively. The reconstruction by linear sampling method and proposed method is shown in Fig. 4(b) and 4(c) respectively. The reconstruction error for LSM and proposed method is 0.7731 and 0.0638 respectively. It can be observed from the results that the LSM fails to accurately detect the location and size of dielectric L-shape objects, whereas CNN reconstructs both dielectric and PEC objects with accurate shape, size, and location. Although CNN reconstruction does not precisely match the original profile, its reconstruction quality is much better than that of LSM as shown in error Tab. 1.

Example 3: In this study, a dielectric cylinder of radius 3 cm centered at (6 cm, –6 cm) along with an U-shape PEC object is taken, as shown in Fig. 5(a). The U-shape object has width and height of 13.5 cm and 5 cm, respectively. The reconstruction by linear sampling method and proposed method is shown in Fig. 5(b) and 5(c) respectively. The reconstruction error for LSM is 0.7775, and for the proposed method, it is 0.0181. Observations from the results are similar to Example 1.

	Error for LSM reconstruction	Error for deep learning assisted LSM reconstruction
Example 1: 2 horizontal dielectric - 1 circular PEC	0.8150	0.0519
Example 2: L shape dielectric - 1 circular PEC	0.7731	0.0638
Example 3: 1 circular dielectric - U shape PEC	0.7775	0.0181
Example 4: 8 circular dielectric - 1 circular PEC	0.7156	0.0106
Example 5: Fresnel experimental data	0.4994	0.0175

Tab. 1. Error for various LSM reconstruction and deep learning assisted LSM reconstruction.

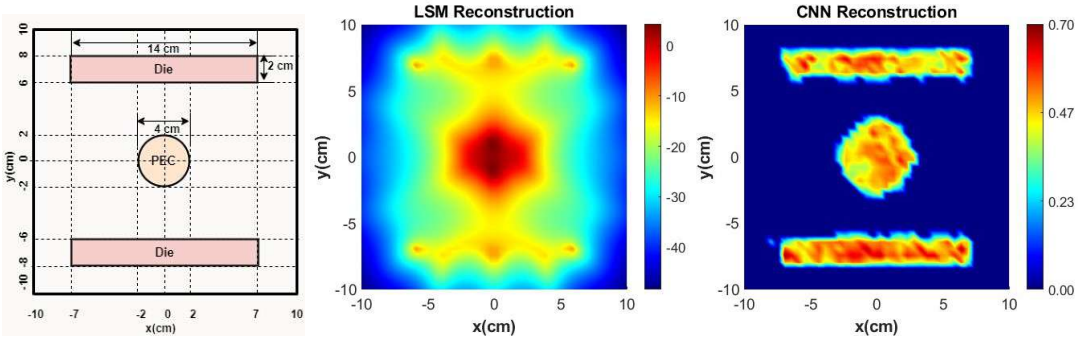

(a) (b) (c)

Fig. 3. Reconstruction result for Example 1 at 3 GHz: (a) Original profile, (b) LSM reconstruction, (c) CNN reconstruction.

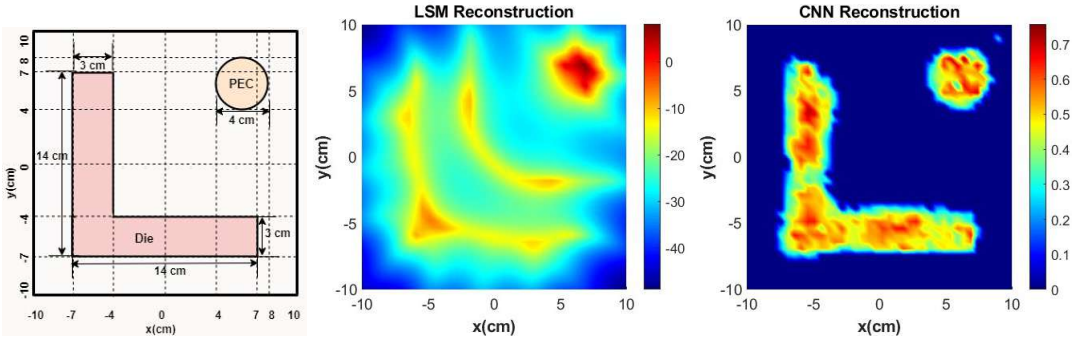

(a) (b) (c)

Fig. 4. Reconstruction result for Example 2 at 3 GHz: (a) Original profile, (b) LSM reconstruction, (c) CNN reconstruction.

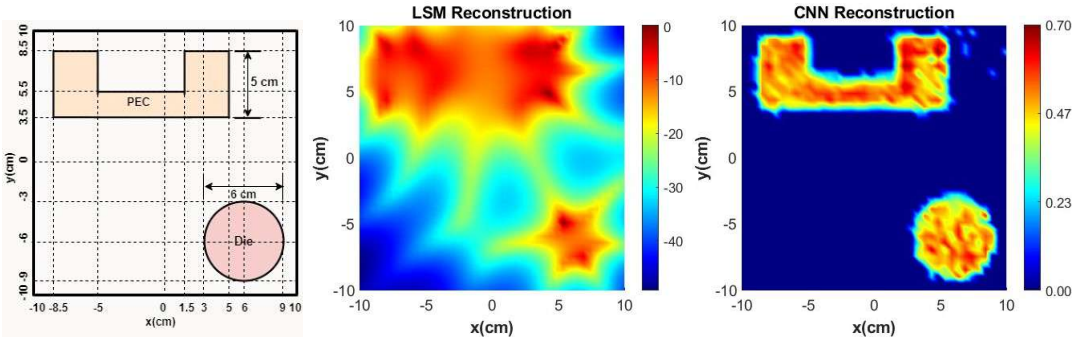

(a) (b) (c)

Fig. 5. Reconstruction result for Example 3 at 3 GHz: (a) Original profile, (b) LSM reconstruction, (c) CNN reconstruction.

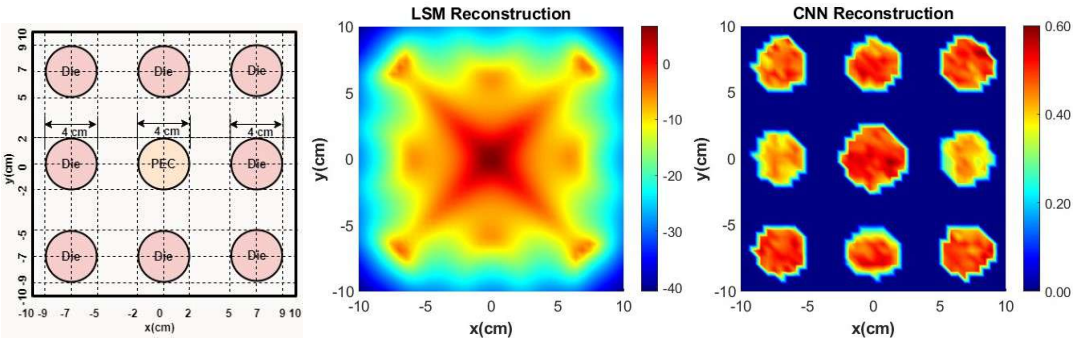

(a) (b) (c)

Fig. 6. Reconstruction result for Example 4 at 3 GHz: (a) Original profile, (b) LSM reconstruction, (c) CNN reconstruction.

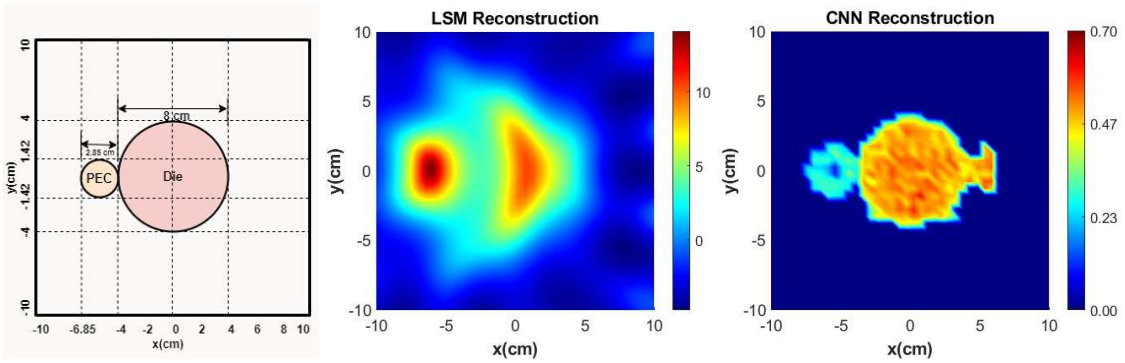

(a) (b) (c)

Fig. 7. Reconstruction result for Example 5 at 3 GHz: (a) Original profile, (b) LSM reconstruction, (c) CNN reconstruction.

Example 4: In this example, eight dielectric cylinders and a PEC cylinder of radius 2 cm each are considered. The cylinders are positioned as shown in Fig. 6(a) The top-left dielectric is centered at (–7 cm, 7 cm), the top-middle dielectric is centered at (0 cm, 7 cm), the top-right dielectric is centered at (7 cm, 7 cm), the middle-left dielectric is centered at (–7 cm, 0 cm), the middle-right dielectric is centered at (7 cm, 0 cm), bottom-left dielectric is centered at (–7 cm, –7 cm), the bottom-middle dielectric is centered at (0 cm, –7 cm), the bottom-right dielectric is centered at (7 cm, –7 cm), and the PEC is centered at origin. The reconstruction by LSM and proposed method is shown in Fig. 6(b) and 6(b) respectively. The reconstruction error for LSM is 0.7156, whereas for the proposed method, it is significantly reduced to 0.0106. The results illustrate that, with a greater number of objects, non linearity increases due to multiple scattering effects, and reconstruction by LSM deteriorates, whereas convolutional neural network reconstruction does not depend on the number of objects, and its reconstruction quality is very good.

Example 5: The proposed method is further validated for experimental data, namely 'FoamMetExt' provided by the Fresnel Institute [20]. It comprises a combination of PEC cylinder with a diameter 2.85 cm and a foam cylinder with a diameter of 8 cm as shown in Fig. 7(a). The relative permittivity of the foam is $\epsilon_r = 1.45$. The experimental test configuration involves a total of 8 transmitters and 241 receivers. The transmitting and receiving antennas were positioned at a distance of 1.67 meters from the centre of the imaging domain. The reconstruction by linear sampling method and proposed method is shown in Fig. 7(b) and 7(c) respectively. The reconstruction error for LSM and proposed method is 0.7731 and 0.0638 respectively. Similar to synthetic examples, the reconstruction of CNN is improved compared to LSM.

Deep learning models [33], such as U-Net, excel in learning hierarchical representations of data through multiple layers of abstraction, enabling them to detect sharp edges in objects effectively. In contrast, LSM relies on explicit mathematical representations to model the scattering phenomenon, which may not encompass all complexities, thus limiting its performance. Additionally, deep learning models inherently operate in a non-linear fashion, allowing them to capture complex relationships between input and output data more effectively. This capability makes them well-suited for segmenting and reconstructing objects with intricate shapes. Conversely, LSM typically relies on linear approximations or assumptions about the scattering process, potentially resulting in inaccuracies, particularly in scenarios where non-linear effects are significant.

3.2 Comparison of Results

Quantitatively the proposed method is compared with recent study [18]. While acknowledging potential disparities in the datasets employed for training and testing between our method and theirs, we identified a commonality in the experimental data, particularly the Fresnel's experimental data 'FoamMetEx.' Through our analysis, we determined that the error associated with our proposed method for the considered experimental data is 0.0175. By comparison, in the aforementioned study [18], the reported errors for PEC and dielectric materials are 0.1718 and 0.1005, respectively, at 3 GHz.

3.3 Low Frequency Characteristics of Linear Sampling Method

The reconstruction quality of the LSM is dependent on the frequency of operation. In this section, analysis is conducted at a low frequency of 200 MHz for various examples, as illustrated in Fig. 8. In the first example, a PEC cylinder of radius 2.5 cm centered at origin and two dielectric strips are considered. Each dielectric strip has length (horizontally) and breadth (vertically) of 2 cm and 12 cm, respectively, and is separated from the PEC object's center by 6.0 cm, as shown in Fig. 8. The second and third examples, as shown in Fig. 8, are the same as Examples 3 and 4

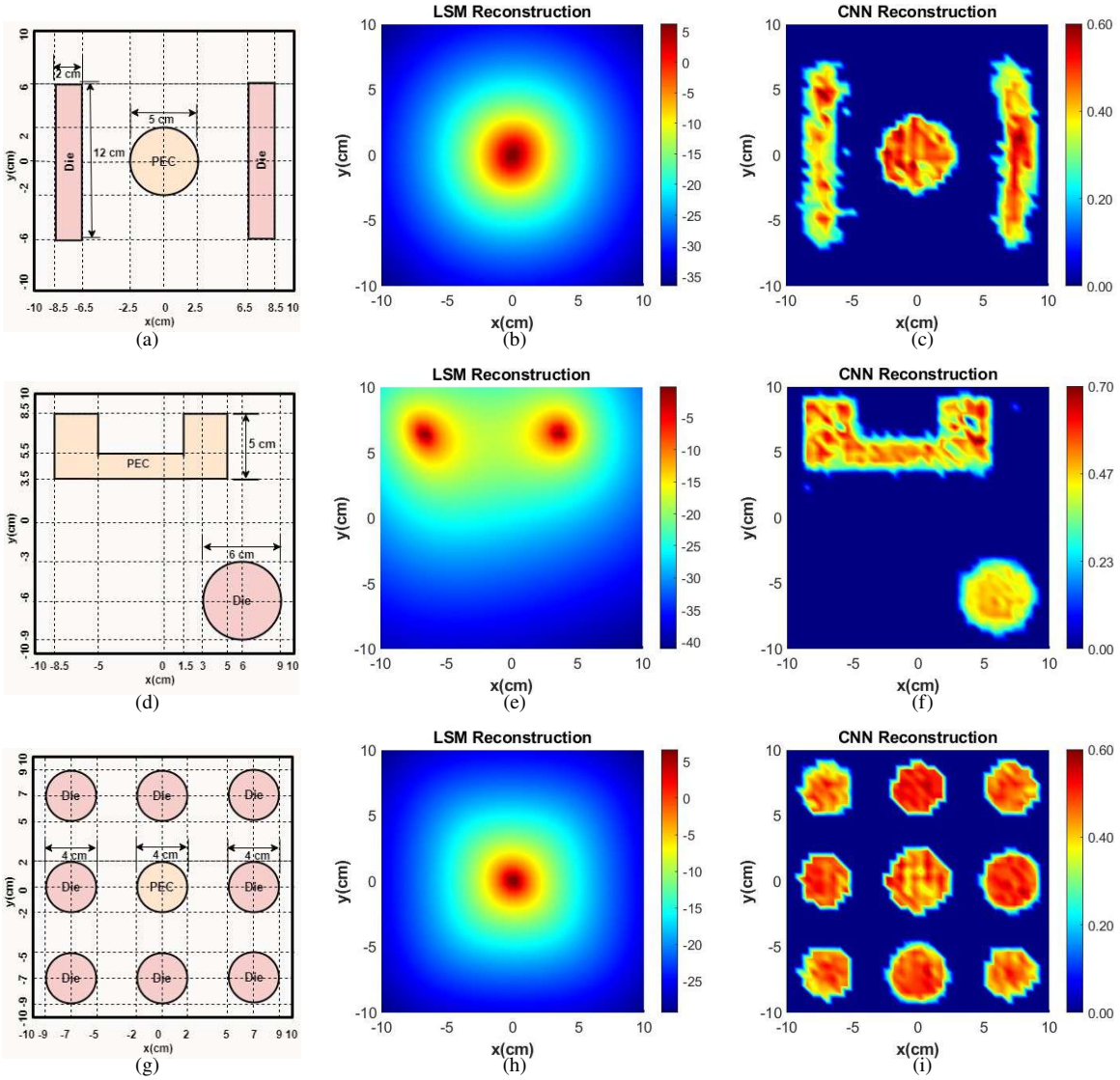

Fig. 8. Reconstruction results at 200 MHz. Original profiles in first column. The second column is LSM reconstruction and CNN reconstruction is in third column.

at 3 GHz, respectively. The reconstructions obtained using LSM and the proposed method is shown in the second and third columns of Fig. 8. The limitation of LSM can be observed from the result, as it fails to detect dielectric at lower frequencies. However, the proposed method reconstructs both dielectric and PEC objects.

3.4 High Frequency Characteristics of Linear Sampling Method

In this section, high frequency characteristic of linear sampling method is analyzed. For this purpose, three examples are considered as shown in Fig. 9. The first example comprises of a PEC cylinder with radius 2 cm centered at origin and two dielectric strips. Each dielectric strip has length (horizontally) and breadth (vertically) of 2 cm and 12 cm, respectively, and is separated from the PEC object's center by 6.5 cm, as shown in Fig. 9. The second and third examples, as shown in Fig. 9, are the same as Examples 3 and 4 at 3 GHz, respectively. The reconstructions obtained using LSM and the proposed method is shown in the second and third columns of Fig. 9. It can be observed from the results that, at higher frequencies, the quality of reconstruction is more deteriorated by LSM, whereas convolutional neural network is able to reconstruct even at higher frequencies.

3.5 Classification of Objects

As discussed in Sec. 3.2, the linear sampling method (LSM) can detect only perfectly electric conducting (PEC) objects at low frequencies, such as 200 MHz. However, at higher frequencies, such as 3 GHz, LSM can detect both dielectric and PEC objects, as noted in Sec. 3.1. These characteristics of conventional LSM are utilized in object classification, as illustrated in Fig. 10.

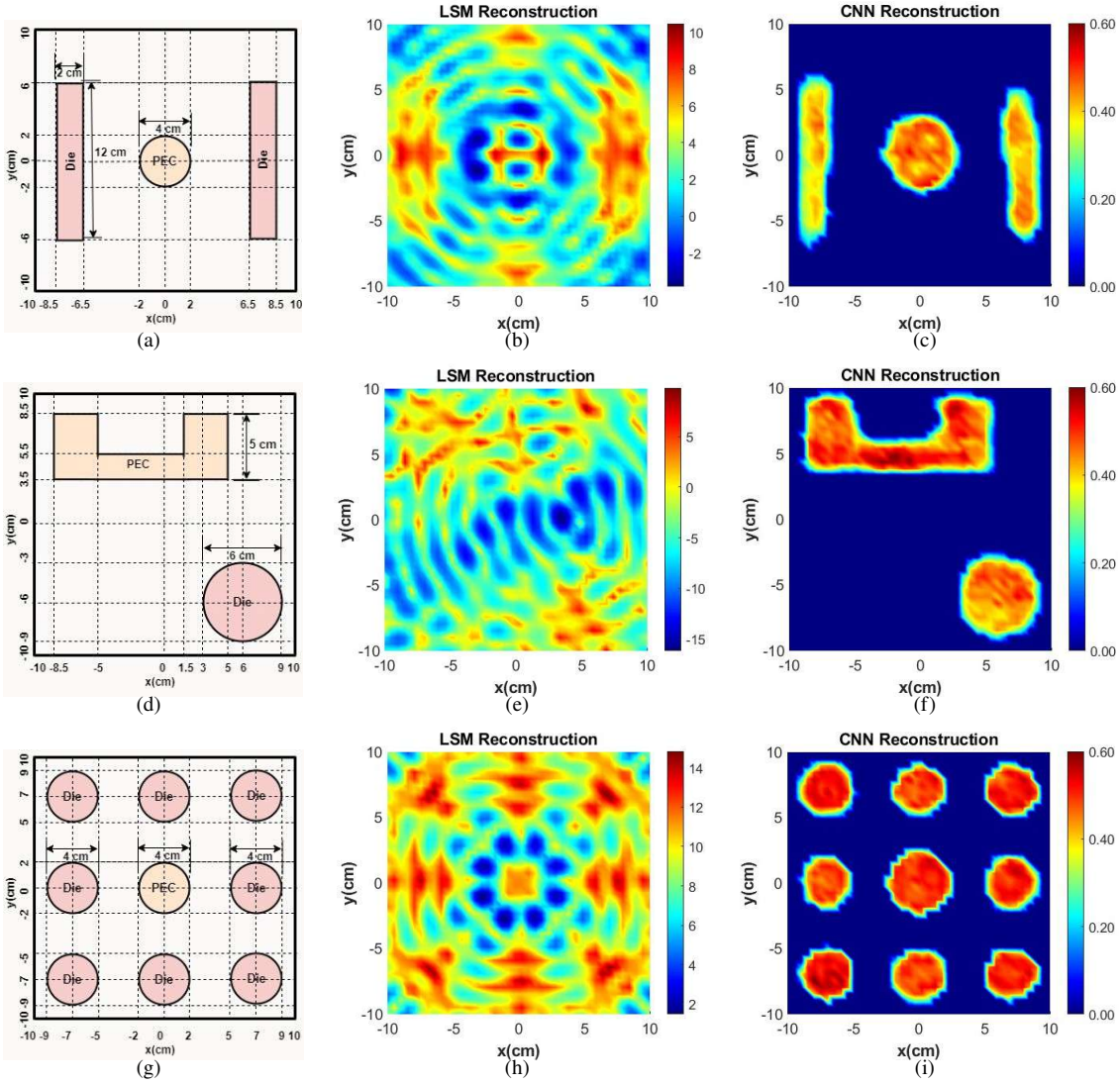

Fig. 9. Reconstruction results at 8 GHz. Original profiles in first column. The second column is LSM reconstruction and CNN reconstruction is in third column.

Object detection is performed using the "regionprops" function in MATLAB, based on a threshold value. This threshold value is calculated as 60% of the mean value of the reconstruction result. Objects with an area of fewer than 15 pixels are discarded. Labeling is accomplished using the "rectangle" function in MATLAB. The classification results are presented for three examples in Figs. 11–13.

Example 1: In this example, three dielectric cylinders and a PEC cylinder of radius 3 cm each are considered. The cylinders are positioned as shown in Fig. 11(a). The top-left dielectric is centered at (–5 cm, 5 cm), the top-right dielectric is centered at (5 cm, 5 cm), the bottom-right dielectric is centered at (5 cm, –5 cm), and the bottom-left PEC is centered at (–5 cm, –5 cm). The linear sampling method reconstruction at 200 MHz with labeling is shown in Fig. 11(b). As discussed in Sec. 3.2, at this frequency, LSM can detect only PEC and labeled in red color. For the same profile, the LSM reconstruction at 3 GHz is fed to trained convolutional neural network (CNN) and the output of CNN with labeling is shown in Fig. 11(c). The CNN output detects four objects. The object closest to the LSM reconstruction at 200 MHz is PEC, while the remaining objects are dielectric. The count of the objects is shown in Fig. 11(d).

Example 2: The geometry of Example 2 (3 GHz results) as depicted in Fig. 12(a) is considered. The reconstructions obtained using LSM at 200 MHz with labeling and the proposed method with classification is shown in Fig. 12(b) and 12(b), respectively. The count of the objects is shown in Fig. 12(d).

Example 3: The geometry of Example 3 (3 GHz results) as depicted in Fig. 13(a) is considered. The reconstructions obtained using LSM at 200 MHz with labeling and the proposed method with classification are shown in Fig. 13(b) and 13(c), respectively. The count of the objects is shown in Fig. 13(d).

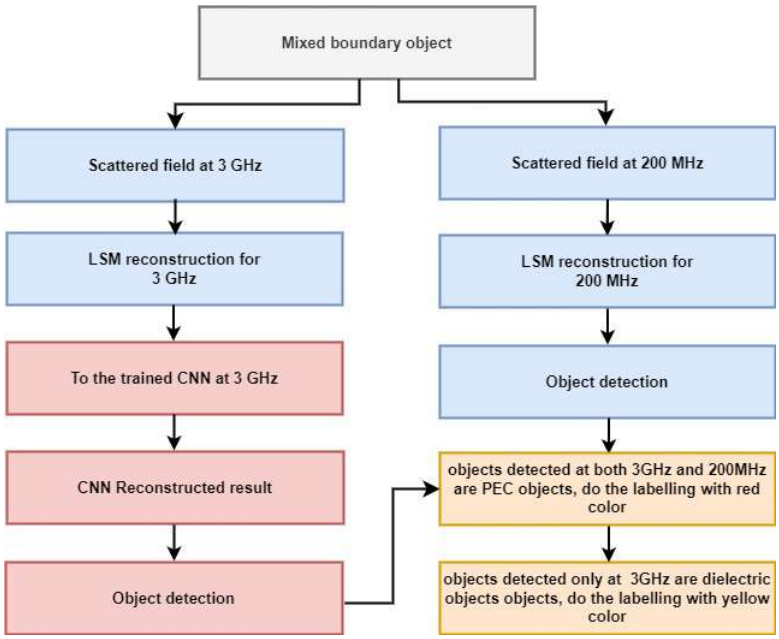

Fig. 10. Process used to classify the mixed boundary objects.

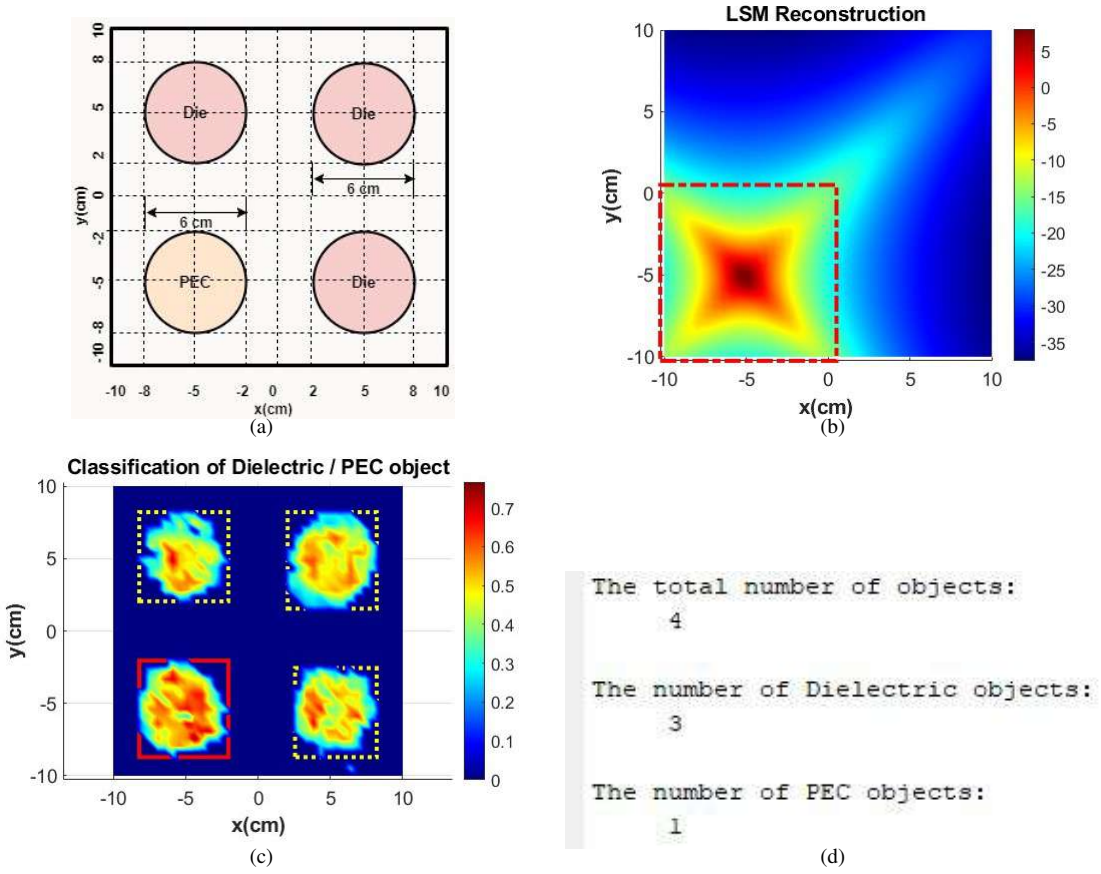

Fig. 11. Classification result for Example 1: (a) Original profile, (b) LSM reconstruction at 200 MHz and labeling, (c) CNN reconstruction at 3 GHz and labeling (red color for PEC and yellow color for dielectric), (d) screen shot of the MATLAB console to display the number of objects.

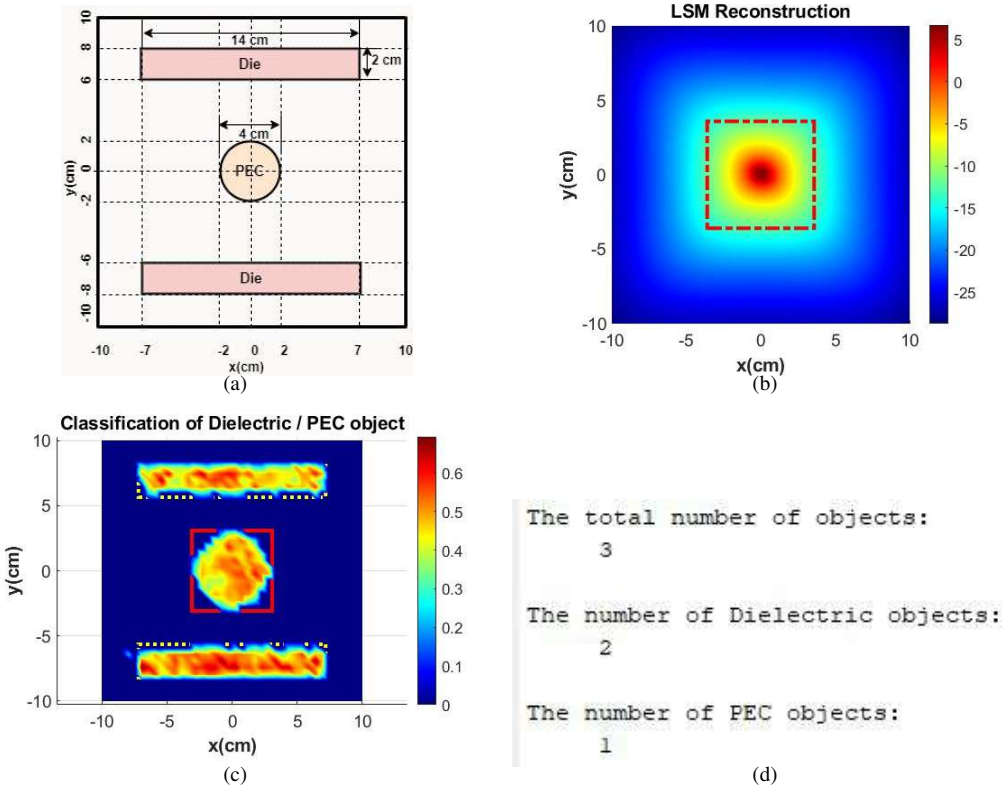

Fig. 12. Classification result for Example 2: (a) Original profile, (b) LSM reconstruction at 200 MHz and labeling, (c) CNN reconstruction at 3 GHz and labeling (red color for PEC and yellow color for dielectric), (d) screen shot of the MATLAB console to display the number of objects.

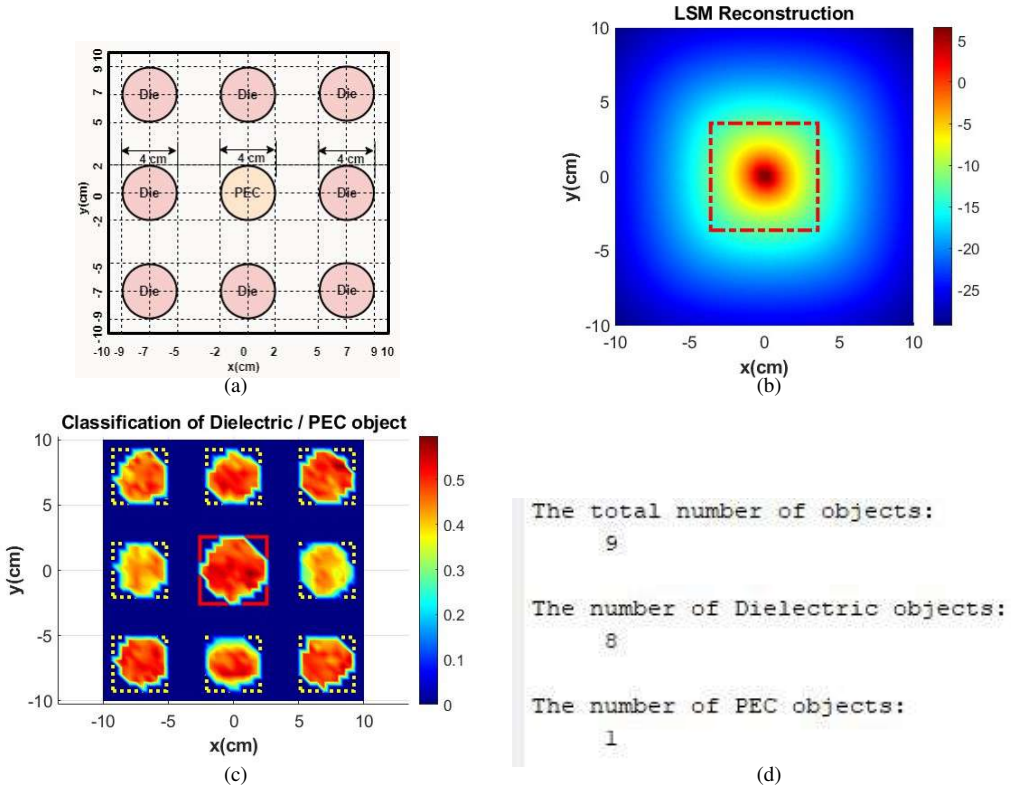

Fig. 13. Classification result for Example 3: (a) Original profile, (b) LSM reconstruction at 200 MHz and labeling, (c) CNN reconstruction at 3 GHz and labeling (red color for PEC and yellow color for dielectric), (d) screen shot of the MATLAB console to display the number of objects.

4. Conclusion

This paper presents a novel approach for reconstructing mixed boundary objects using a deep learning-assisted linear sampling method. The employed architecture is the U-Net, where the LSM provides an initial estimate that is input to the convolutional neural network for further refinement. In order to train the network, various mixed objects in the shapes of circular cylinders, rectangles, L-shapes, and U-shapes are generated. After that, a variety of examples, including synthetic and experimental datasets, are used to test the trained model. The LSM limitations like its inability to detect dielectric objects at low frequency and quality of reconstruction deteriorates significantly at very high frequencies, is addressed by deep learning assisted linear sampling method. Finally, classification of objects is demonstrated through various examples. Future works in this direction is to explore the 2-D-TE and 3-D cases of illumination.

Acknowledgments

The research work carried out in this paper is supported by the Core Research Grant, SERB, India, File No. CRG/2020/004127.

References

[1] PASTORINO, M. *Microwave Imaging*. John Wiley & Sons, 2010. ISBN: 9780470278000

[2] NIKOLOVA, N. K. *Introduction to Microwave Imaging*. Cambridge University Press, 2017. ISBN: 9781316084267

[3] COLTON, D., HADDAR, H., PIANA, M. The linear sampling method in inverse electromagnetic scattering theory. *Inverse Problems*, 2003, vol. 19, no. 6, p. 105–137. DOI: 10.1088/0266-5611/19/6/057

[4] COLTON, D., MONK, P. Target identification of coated objects. *IEEE Transactions on Antennas and Propagation*, 2006, vol. 54, no. 4, p. 1232–1242. DOI: 10.1109/TAP.2006.872564

[5] CATAPANO, I., CROCCO, L., ISERNIA, T. Improved sampling methods for shape reconstruction of 3-D buried targets. *IEEE Transactions on Geoscience and Remote Sensing*, 2008, vol. 46, no. 10, p. 3265–3273. DOI: 10.1109/TGRS.2008.921745

[6] CATAPANO, I., CROCCO, L. An imaging method for concealed targets. *IEEE Transactions on Geoscience and Remote Sensing*, 2009, vol. 47, no. 5, p. 1301–1309. DOI: 10.1109/TGRS.2008.2010773

[7] CATAPANO, I., SOLDOVIERI, F., CROCCO, L. On the feasibility of the linear sampling method for 3-D GPR surveys. *Progress In Electromagnetics Research*, 2011, vol. 118, p. 185–203. DOI: 10.2528/PIER11042704

[8] CATAPANO, I., CROCCO, L. A qualitative inverse scattering method for through-the-wall imaging. *IEEE Geoscience and Remote Sensing Letters*, 2010, vol. 7, no. 4, p. 685–689. DOI: 10.1109/LGRS.2010.2045473

[9] BOZZA, G., BRIGNONE, M., PASTORINO, M. Application of the no-sampling linear sampling method to breast cancer detection. *IEEE Transactions on Antennas and Propagation*, 2010, vol. 57, no. 10, p. 2525–2534. DOI: 10.1109/TBME.2010.2055059

[10] AKDUMAN, I., JANJIC A, BUGDAYCI, O., et al. SAFE: A microwave imaging device for breast cancer early screening. *European Journal of Cancer*, 2022, vol. 175, no. 1, p. 32–33. DOI: 10.1016/S0959-8049(22)01435-6

[11] ERRAMSHETTY, M., BHATTACHARYA, A. Shape reconstruction of mixed boundary objects by linear sampling method. *IEEE Transactions on Antennas and Propagation*, 2015, vol. 63, no. 7, p. 3077–3086. DOI: 10.1109/TAP.2015.2426679

[12] MASSA, A., MARCANTONIO, D., CHEN, X., et al. DNNs as applied to electromagnetics, antennas, and propagation - A review. *IEEE Antennas and Wireless Propagation Letters*, 2019, vol. 18, no. 11, p. 2225–2229. DOI: 10.1109/LAWP.2019.2916369

[13] CHEN, X., WEI, Z., LI, M., et al. A review of deep learning approaches for inverse scattering problems (invited review). *Progress in Electromagnetics Research*, 2020, vol. 167, p. 67–81. DOI: 10.2528/PIER20030705

[14] ARREBOLA, M., LI, M., SALUCCI, M. Guest editorial artificial intelligence: New frontiers in real-time inverse scattering and electromagnetic imaging. *IEEE Transactions on Antennas and Propagation*, 2022, vol. 70, no. 8, p. 6131–6134. DOI: 10.1109/TAP.2022.3198305

[15] BENNY, R., ANJIT, T. A., MYTHILI, P. Deep learning based non-iterative solution to the inverse problem in microwave imaging. *Progress in Electromagnetics Research M*, 2022, vol. 109, p. 231–240. DOI: 10.2528/PIERM22010905

[16] YAGO RUIZ, Á., CAVAGNARO, M., CROCCO, L. An effective framework for deep-learning-enhanced quantitative microwave imaging and its potential for medical applications. *Sensors*, 2023, vol. 23, no. 2, p. 1–16. DOI: 10.3390/s23020643

[17] KUO, Y. H., KIANG, J. F. Deep-learning linear sampling method for shape restoration of multilayered scatterers. *Progress in Electromagnetics Research C*, 2022, vol. 124, p. 197–209. DOI:10.2528/PIERC22081005

[18] SONG, R., HUANG, Y., YE, X., et al. Learning-based inversion method for solving electromagnetic inverse scattering with mixed boundary conditions. *IEEE Transactions on Antennas and Propagation*, 2022, vol. 70, no. 8, p. 6218–6228. DOI: 10.1109/TAP.2021.3139645

[19] ZHANG, Q. Q., CHENG, Y. Y., AN, Q. L., et al. An inverse scattering reconstruction method for perfect electric conductor-dielectric hybrid target based on physics-inspired network. *IET Radar Sonar Navigation*, 2023, vol. 17, no. 8, p. 1286–1298. DOI: 10.1049/rsn2.12419

[20] GEFFRIN, J. M., SABOUROUX, P., EYRAUD, C. Free space experimental scattering database continuation: Experimental set-up and measurement precision. *Inverse Problems*, 2005, vol. 21, no. 6, p. 117–130. DOI: 10.1088/0266-5611/21/6/S09

[21] COLTON, D., KRESS, R. *Inverse Acoustic and Electromagnetic Scattering Theory*. Berlin (Germany): Springer, 1992. DOI: 10.1007/978-1-4614-4942-3

[22] PETERSON, A. F., RAY, S. L., MITTRA, R. *Computational Methods for Electromagnetics*. New York (USA): Oxford University Press, 2001. ISBN: 9780780311220

[23] RICHMOND, J. H. Scattering by a dielectric cylinder of arbitrary cross section shape. *IEEE Transactions on Antennas and Propagation*, 1965, vol. 13, no. 3, p. 334–341. DOI: 10.1109/TAP.1965.1138427

[24] BERTERO, M., BOCCACCI, P. *Introduction to Inverse Problems in Imaging*. Bristol (U.K.): IOP Publishing Ltd., 1998. DOI: 10.1201/9781003032755

[25] COLTON, D., HADDAR, H. An application of the reciprocity gap functional to inverse scattering theory. *Inverse Problems*, 2005, vol. 21, no. 1, p. 383–398. DOI: 10.1088/0266-5611/21/1/023

[26] CATAPANO, I., CROCCO, L., ISERNIA, T. On simple methods for shape reconstruction of unknown scatterers. *IEEE Transactions on Antennas and Propagation*, 2007, vol. 55, no. 5, p. 1431–1435. DOI: 10.1109/TAP.2007.895563

[27] BRIGNONE, M., BOZZA, G., ARAMINI, R., et al. A fully no-sampling formulation of the linear sampling method for three-dimensional inverse electromagnetic scattering problems. *Inverse Problems*, 2009, vol. 25, no. 1, p. 1–20. DOI: 10.1088/0266-5611/25/1/015014

[28] JIN, K. H., MCCANN, M. T., FROUSTEY, E., et al. Deep convolutional neural network for inverse problems in imaging. *IEEE Transactions on Image Processing*, 2017, vol. 26, no. 9, p. 4509–4522. DOI: 10.1109/TIP.2017.2713099

[29] HARISHA, S. B., MALLIKARJUN, E., AMIT, M. Deep learning assisted linear sampling method for the reconstruction of perfect electric conductors. *Radioengineering*, 2024, vol. 33, no. 1, p. 89–99. DOI: 10.13164/re.2024.0089

[30] RONNEBERGER, O., FISCHER, P., BROX, T. U-net: Convolutional networks for biomedical image segmentation. In *International Conference on Medical Image Computing and Computer-Assisted Intervention (MICCAI)*. Munich (Germany), 2015, p. 234–241. DOI: 10.1007/978-3-319-24574-4_28

[31] AGARWAL, K., CHEN, X., ZHONG, Y. A multipole-expansion based linear sampling method for solving inverse scattering problems. *Optics Express*, 2010, vol. 18, no. 6, p. 6366–6381. DOI: 10.1364/OE.18.006366

[32] BURFEINDT, M. J., ALQADAH, H. F. Qualitative inverse scattering for sparse-aperture data collections using a phase-delay frequency variation constraint. *IEEE Transactions on Antennas and Propagation*, 2020, vol. 68, no. 11, p. 7530–7540. DOI: 10.1109/TAP.2020.2998217

[33] GOODFELLOW, I., BENGIO, Y., COURVILLE, A. *Deep Learning*. MIT Press, 2016. [Online]. Available at: http://www.deeplearningbook.org

About the Authors . . .

Shimoga Beerappa HARISHA (corresponding author) has received his M.Tech. from the National Institute of Technology Warangal in 2009. He is currently pursuing a Ph.D. degree at the National Institute of Technology Goa. His research interests include microwave imaging, inverse problems and deep learning.

Erramshetty MALLIKARJUN has received his M.Tech. and Ph.D. degrees from the Indian Institute of Technology Kharagpur in 2009 and 2016, respectively. Currently, he is an Assistant Professor with the National Institute of Technology Goa. His fields of interest include microwave imaging, terahertz imaging, inverse problems and deep learning.

Magdum AMIT has received his M.Tech. from Walchand College of Engineering Sangli in 2016 and Ph.D. degree from the National Institute of Technology Goa in 2023. His research interests include microwave imaging, inverse problems and deep learning.